Journal of the American College of Cardiology
© 1999 by the American College of Cardiology
Published by Elsevier Science Inc.

Vol. 33, No. 3, 1999
ISSN 0735-1097/99/$20.00
PII S0735-1097(98)00627-5

Chordal Force Distribution Determines Systolic Mitral Leaflet Configuration and Severity of Functional Mitral Regurgitation

Sten Lyager Nielsen, MD,*† Hans Nygaard, DMSc,*† Arnold A. Fontaine, PhD,‡ J. Michael Hasenkam, MD, DMSc,*† Shengqui He, MD,‡ Niels T. Andersen, PhD,§ Ajit P. Yoganathan, PhD‡

Aarhus, Denmark and Atlanta, Georgia

OBJECTIVES The purpose of this study was to investigate the impact of the chordae tendineae force distribution on systolic mitral leaflet geometry and mitral valve competence in vitro.

BACKGROUND Functional mitral regurgitation is caused by changes in several elements of the valve apparatus. Interaction among these have to comply with the chordal force distribution defined by the chordal coapting forces (F_C) created by the transmitral pressure difference, which close the leaflets and the chordal tethering forces (F_T) pulling the leaflets apart.

METHODS Porcine mitral valves (n = 5) were mounted in a left ventricular model where leading edge chordal forces measured by dedicated miniature force transducers were controlled by changing left ventricular pressure and papillary muscle position. Chordae geometry and occlusional leaflet area (OLA) needed to cover the leaflet orifice for a given leaflet configuration were determined by two-dimensional echo and reconstructed three-dimensionally. Occlusional leaflet area was used as expression for incomplete leaflet coaptation. Regurgitant fraction (RF) was measured with an electromagnetic flowmeter.

RESULTS Mixed procedure statistics revealed a linear correlation between the sum of the chordal net forces, $\Sigma[F_C - F_T]_s$, and OLA with regression coefficient (minimum − maximum) beta = −115 to −65 [mm^2/N]; $p < 0.001$ and RF (beta = −0.06 to −0.01 [%/N]; $p < 0.001$). Increasing F_T by papillary muscle malalignment restricted leaflet mobility, resulting in a tented leaflet configuration due to an apical and posterior shift of the coaptation line. Anterior leaflet coapting forces increased due to mitral leaflet remodeling, which generated a nonuniform regurgitant orifice area.

CONCLUSIONS Altered chordal force distribution caused functional mitral regurgitation based on tented leaflet configuration as observed clinically. (J Am Coll Cardiol 1999;33:843–53) © 1999 by the American College of Cardiology

Significant mitral valve regurgitation (MR) without structural tissue defect is observed in 11% of patients undergoing coronary angiography due to coronary artery disease (1). Since MR has an impact on the long-term prognosis after myocardial revascularization (2), recognition of its precise etiology may be helpful in identifying rational corrective procedures that also improve left ventricular function.

Typically, these patients have normal leaflets that are displaced apically, resulting in incomplete mitral leaflet coaptation (3). Despite extensive characterization of the phenomenon, the precise mechanism remains unclear. Several points of view have been adopted, each providing a seemingly rational explanation of functional MR. With the exception of intrinsic papillary muscle dysfunction (4), the majority have implicated a component of left ventricular remodeling as the primary determinant of MR (3,5–11). However, global left ventricular dysfunction is often accompanied by multiple alterations of the mitral valve apparatus, any of which can lead to MR (11). Nevertheless, interaction among the mitral valve components has to comply with the concept of the chordal force distribution defined by the chordal coapting forces created by the transmitral pressure difference, which close the mitral leaflets and the chordal tethering forces tending to pull the leaflets apart (12).

In the present in vitro study, we tested the hypothesis that functional MR is directly related to an altered balance between the chordal coapting and chordal tethering forces

From the *Department of Cardiothoracic and Vascular Surgery, and †Institute of Experimental Clinical Research, Skejby Sygehus, Aarhus University Hospital, Aarhus, Denmark; ‡Institute for Bioengineering Bioscience and School of Chemical Engineering, Georgia Institute of Technology, Atlanta, Georgia, and §Institute of Biostatistics, Aarhus University, Aarhus, Denmark. This project has been financially supported by grants from the Danish Heart Foundation (96-1-3-58-22370; 96-2-2-20-22417), The Danish Medical Research Council and the Research Initiative of Aarhus University Hospital.

Manuscript received July 27, 1998; revised manuscript received September 18, 1998, accepted November 18, 1998.

Abbreviations and Acronyms

APL	=	apical posterolateral
APM	=	anterolateral papillary muscle
D_{AL}, D_{PL}	=	distance from the anterior/posterior leaflet tip to the annular plane
F_C, F_T	=	chordal coapting and tethering force component. Subscripts AA, AP, PA, PP refer to chordae location (chordae from APM to the anterior leaflet, from APM to the posterior leaflet, from PPM to the anterior leaflet and from PPM to the posterior leaflet). Subscripts APM and PPM refer to the chordal forces emanating from APM and PPM. Subscripts AL and PL refer to the chordal forces supplying the anterior and posterior leaflet. Subscript S refers to the sum of the chordal force components
L_{AL}, L_{PL}	=	horizontally projected anterior and posterior leaflet length
L_{APM}, L_{PPM}, L_{PM}	=	papillary muscle lengths (distance from APM/PPM tip to the annular plane through the midpoint of the corresponding half mitral systolic coaptation point). L_{PM} is the mean of L_{APM} and L_{PPM}
LVP − LAP	=	transmitral pressure difference
MR	=	mitral valve regurgitation
OLA	=	occlusional leaflet area of the mitral valve. Subscript ACOM/PCOM refers to the anterolateral/posteromedial commissural half portion
PPM	=	posteromedial papillary muscle
RF	=	mitral regurgitant fraction
2D	=	two-dimensional
α_{AL}, α_{PL}	=	coaptation angle of the anterior/posterior leaflet
φ_{AL}, φ_{PL}	=	anterior/posterior leaflet excursion angle

in ventricular systole. Therefore, the aim of the study was to investigate the impact of the chordal force distribution on systolic mitral leaflet configuration and severity of MR.

METHODS

In Vitro Model. The experiments were conducted in a left heart simulator, comprising a computer-controlled, pressure-driven compressible bladder type pulsatile pump system (13). Hemodynamic conditions could be simulated at heart rates from 40 to 160 min^{-1}, and cardiac output up to 10 liter/min with physiologic pressure and flow wave forms. A 0.9% saline solution was used as blood analog fluid.

The measurements were conducted in a rigid left ventricular model with dimensions of the human left ventricle at the onset of systole (Fig. 1). The model allowed independent adjustment of the papillary muscle positions over a clinically relevant range (Fig. 2).

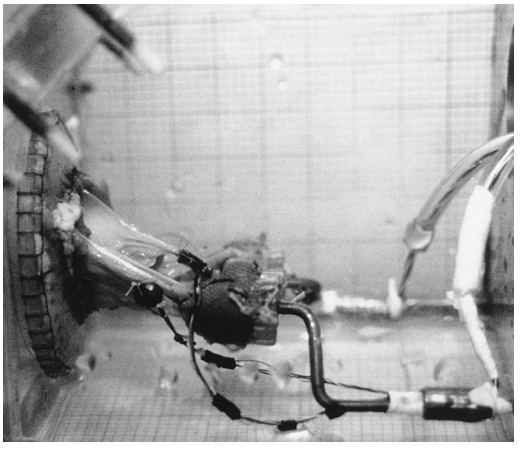

Figure 1. Photograph of the left ventricular model showing the mitral valve mounting mechanism consisting of an annulus ring and two papillary muscle mounting rods. Chordal force transducers were attached to the primary (major fixing) chordae.

A transparent millimetric foil placed on the model allowed readings of three-dimensional coordinates, where x referred to the horizontal plane, y to the sagittal plane and z to the axial plane. The centerpoint of the inner rigid annular ring was defined as origo (0,0,0). In this system the mitral valve structures could be characterized three-dimensionally.

VALVES. Porcine mitral valves with intact chordae tendineae and papillary muscles with an intertrigonal distance of 25 mm were tested in the model. The valves were slightly fixated in 1% glutaraldehyde solution to prolong the tissue integrity of the valve. Each valve had a total leaflet surface area that was nearly twice that of the annular ring area, which is similar to the ratio of normal human mitral valves (14). The number and distribution of the chordae tendineae in the porcine mitral valve are similar to human mitral valves (15). The native mitral annulus was mounted on an inner ellipsoid ring that was attached to a rigid round outer ring by a waterproof Dacron cloth stretched tightly between the two rings. The anatomic shape and size of the inner annulus were determined by mitral valve sizers used by surgeons for sizing of mitral annuloplasty rings (Medtronic Inc.). The outer ring was mounted on the atrial section of the model, so the anterior leaflet was positioned anteriorly between the mitral orifice and the left ventricular outflow tract.

The papillary muscles were wrapped in a Dacron cuff for support and then sutured to sewing disks on the ends of sigmoidal mounting rods, shown in Figure 1. Although the posteromedial and the anterolateral papillary muscles have been designed anatomically, they both lie in the posterior half of the left ventricle with a line joining the tips running parallel to the coaptation line of the mitral leaflets (3). In our model the medial scallop of the posterior leaflet was positioned posteriorly opposite to the anterior leaflet in the sagittal plane. Therefore, to simulate the papillary muscle displacement that can occur in ischemic heart disease or

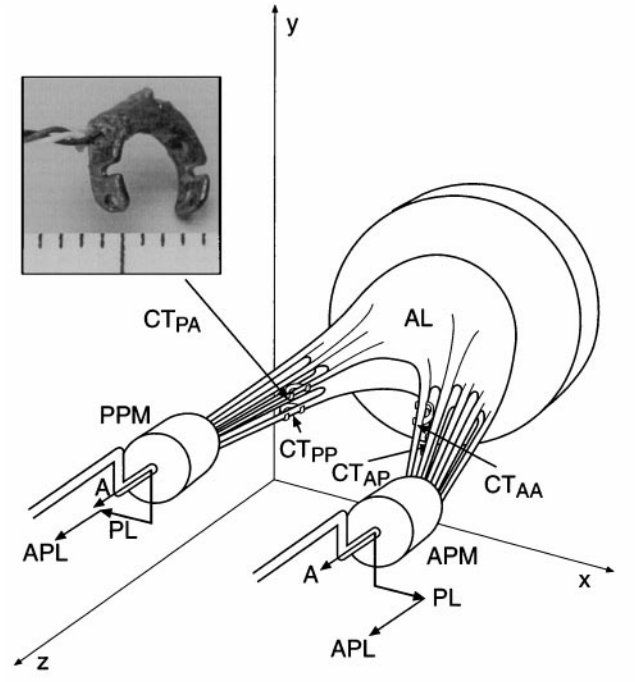

Papillary muscle settings

	1	2	3	4	5	6	7	8
APM	N	A	N	N	PL	PL	APL	APL
PPM	N	A	PL	APL	PL	APL	PL	APL

Figure 2. Schematic showing the distribution of the chordal force transducers and the papillary muscle adjustments in normal (N), apical (A), posterolateral (PL) and apical posterolateral (APL) directions. Eight papillary muscle settings were tested. Scaled photograph of the transducer: 1 unit = 1 mm. CT_{AA} = chorda from the anterolateral papillary muscle (APM) to anterior leaflet; CT_{AP} = chorda from APM to posterior leaflet; CT_{PA} = chorda from the posteromedial papillary muscle (PPM) to anterior leaflet; CT_{PP} = chorda from PPM to posterior leaflet; AL = anterior leaflet.

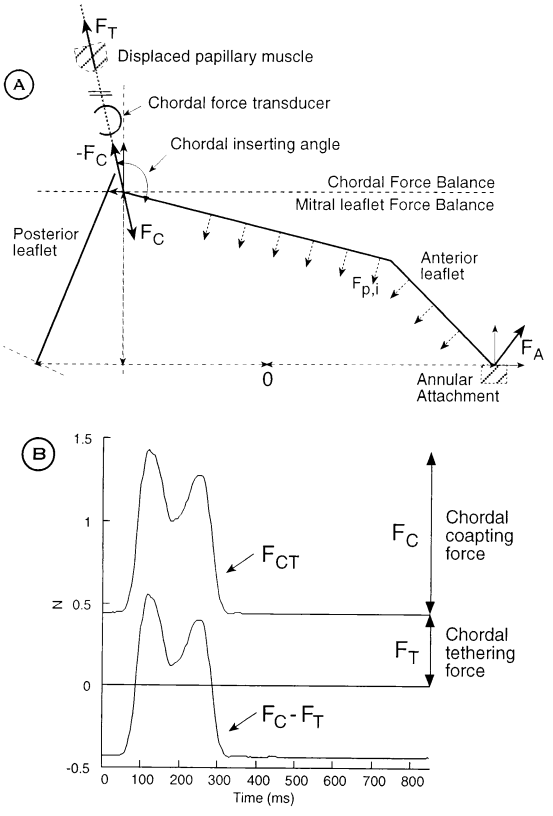

Figure 3. (A) Free body diagram of the mitral valve complex. In an equilibrium condition of the closed mitral valve complex in systole, mitral leaflet force balance (below the **dashed line**) requires that the transmitral pressure forces ($F_{P,i}$) are counteracted by the chordal tethering force, F_T (equal to $-F_C$) and the annular tethering force, F_A. Chordal force balance (above the **dashed line**) requires that the coapting force component F_C is counteracted by an equal and oppositely directed tethering force from the papillary muscle attachment, F_T. Transmitral pressure forces and F_A are only presented for schematic and conceptual purposes and were not assessed in the study. **(B)** The chordal force measure of each chorda tendinea consisted of the chordal tethering force component (F_T) and the chordal coapting force component (F_C). The difference of the force components, ($F_C - F_T$), defined the resulting (valvular directed) force of the chorda tendinea acting on the leaflets at the point of insertion.

dilated cardiomyopathy (8), the papillary muscles were retracted in apical (A), posterolateral direction (PL) and apical posterolateral (APL) directions (Fig. 2).

MEASUREMENTS

Chordae tendineae forces. Specially self-designed chordal force transducers were directly attached to the chordae tendineae of the mitral valve. Each transducer was constructed of a C-shaped copper ring, 6 mm in diameter and 0.8 mm thick (Fig. 2). Two miniature strain gauges (model EA-06-031DE-350, Measurements Group, Raleigh, North Carolina) were glued to the inner and outer surface of the ring, coated and coupled in a Wheatstone half-bridge to a strain gauge indicator (model 1526, Brüel & Kjaer, Copenhagen, Denmark). Before use in the model, the transducers were individually calibrated and tested for sensitivity, hysteresis and linearity to force units in a range of 0 to 5 N and for electrical stability in a 0.9% saline solution. In each end of the C-template a thin slit and two small holes were incorporated to permit fixation of a chorda tendinea with a Prolene 6-0 suture. After fixation, the chordal fiber was cut between the two ends of the transducer.

In each valve, four chordal force transducers were fixated to the marginal branch of the major fixing primary chordae tendineae (16) (Fig. 2).

The force transducers measured the resulting force on each chorda tendinea representing the sum of the tethering force component (F_T) directed toward the papillary muscles, and the coapting force component (F_C) directed toward the leaflets (Fig. 3). The chordal tethering and coapting force components were both projected along the chorda; each of them increased the chordal tension. Since the papillary muscles were fixated to static mounting rods, the chordal tethering force reflected the force measurement during left

ventricular diastole, when there was no pressure difference between the left ventricle and the left atrium. The chordal tethering force was assumed to be zero when the papillary muscles were in the normal position, and thus F_T for a given papillary muscle setting was calculated by subtracting the observed F_T with the papillary muscles in normal position from the F_T when the papillary muscles were displaced. The chordal coapting force was the increase in the chordal force measurement when the left ventricular pressure was applied to close the valve. The difference between the coapting and tethering force component ($F_C - F_T$) of each chorda defined the resultant force that determined leaflet position at the point of insertion.

The spatial orientation of the chordae connecting the papillary muscle tip and the midpoint of the corresponding half mitral systolic coaptation line were determined by two-dimensional (2D) echocardiographic (see below). Hence, the measured chordal forces could be resolved into x (horizontal), y (sagittal) and z (axial) components: $F_T(x)$, $F_T(y)$, $F_T(z)$, $F_C(x)$, $F_C(y)$, $F_C(z)$.

Theoretically, the total chordal force balance is given by the vector summation of the tethering and coapting force vectors of all the chordae supporting the anterior and posterior leaflet (12). Using only four chordal force transducers, we could not actually measure the total chordal force balance. However, we anticipate that relative changes of the chordal force distribution were reflected by our measurements and could be used to interpret the relation between leaflet configuration and the overall chordal force distribution.

Hemodynamics. The transmitral pressure difference (LVP − LAP) was measured by a differential pressure transducer (model DP15 TL, Validyne Inc., Northridge, CA) coupled to an amplifier/signal conditioner (model CD12 A-1-A, Validyne Inc., Northridge, California).

Transmitral flow rates were measured in the left atrium 4 cm upstream of the valve by an electromagnetic cannular flow probe with a 25.4-mm internal bore (model EP680, Carolina Medical Instruments Inc., King, North Carolina), coupled to an analog flowmeter (model FM 501, Carolina Medical Instruments Inc., King, North Carolina).

Mitral valve imaging. Two-dimensional echocardiographic recordings were made with a phased array ultrasound sector scanner (Sonolayer SSA-270A, Toshiba Inc.) using a 3.75-MHz probe (PSF-37DT). Machine settings were adjusted to provide optimal imaging with the highest possible frame rate at a penetration depth of 12 cm.

The ultrasound transducer was positioned at the apex of the left ventricular model and rotated counterclockwise from the horizontal plane (0°) in 45° steps. Thus, 2D echocardiographic recordings from four different scanning planes were obtained: 1) 0°, 2) 45°, 3) 90° (apical long-axis view) and 4) 135° (apical four-chamber view). In addition, 2D echocardiographic recordings were obtained from parasternal long-axis and short-axis views. All echocardiographic data were recorded on videotape, and representative heart cycles were later transferred synchronized with the transmitral flow curve to a computer for off-line analysis in a commercially available software program (EchoPAC, VingMed, Norway).

Data Analysis

Transmitral pressure difference, mitral flow, chordal force and pump trigger signals were stored on a tape recorder (TEAC RD 180T PCM, Teac Corp., Japan) for off-line analysis on a computer after analog-to-digital conversion with a sample frequency of 300 Hz. By a dedicated software program (designed in LabVIEW 4.01), one mean pump cycle from each channel was obtained by ensemble averaging 10 pump cycles.

Chordae tendineae forces. Peak chordal F_C and F_T were assessed from the chordal force signals. Coapting force component and F_T were resolved into x,y,z vectors knowing the orientation of the chordae (see below). The magnitude of the total chordal net force, $\Sigma[F_C - F_T]_S$, the chordal net force of anterior leaflet, $\Sigma[F_C - F_T]_{AL}$, and posterior leaflet, $\Sigma[F_C - F_T]_{PL}$, and from anterolateral papillary muscle, $\Sigma[F_C - F_T]_{APM}$, and posteromedial papillary muscle, $\Sigma[F_C - F_T]_{PPM}$, were determined as the sum of the square root square of $\Sigma[F_C - F_T](x)$, $\Sigma[F_C - F_T](y)$ and $\Sigma[F_C - F_T](z)$ of the respective chordae.

Hemodynamics. Early systolic peak + (LV − LA) dP/dt were computed from the LVP − LAP pressure recordings.

From the transmitral flow data the following parameters were calculated: forward flow volume, regurgitant flow volume, stroke volume and mitral regurgitant fraction (RF). The closing volume represented the fluid displaced by the valve during closure. The precoaptation regurgitant volume was defined as the difference between the measured closing volume in the test condition and the closing volume of the same valve for the normal papillary muscle position and same physiologic condition.

Mitral valve imaging. Echocardiographic data were used to assess mitral leaflet mobility and systolic leaflet configuration.

LEAFLET COAPTATION. In each apical view, the following parameters were measured (Fig. 4): the perpendicular projected distance from the annular plane to the anterior and posterior leaflet tip (D_{AL} and D_{PL}); the projected length of the leaflets (L_{AL} and L_{PL}); the leaflet coaptation angle (α_{AL} and α_{PL}), and the leaflet excursion angle, which was defined as the angle through which each leaflet travelled (φ_{AL} and φ_{PL}; not shown). Except for leaflet excursion angle, only one representative early midsystolic frame per view was analyzed.

OCCLUSIONAL LEAFLET AREA. The occlusional leaflet area (OLA) was defined as the leaflet surface area required to cover the mitral orifice for a given leaflet geometry orienta-

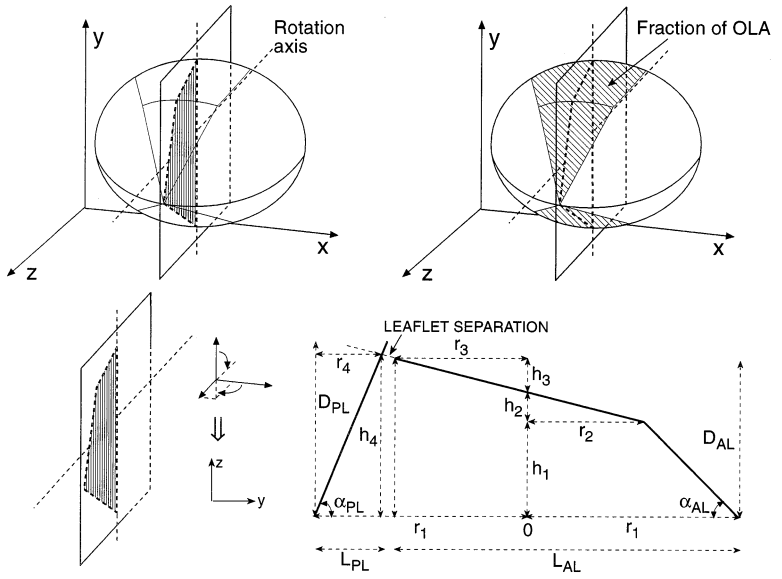

Figure 4. Diagram of a midsystolic tented mitral leaflet geometry **(left top)** with a typical leaflet contour imaged by two-dimensional echo from the apical view **(below)**. Left ventricular side in z direction. The occlusional leaflet area, OLA, was calculated as the sum of fractions of a cone produced from four apical scanning planes rotated around an axis through the midpoint of the annulus (**right top**; one fraction of a cone is marked). Notice leaflet edge separation due to leaflet asynergy creating a regurgitant orifice. Variables to describe leaflet configuration are illustrated (r and h). The intersection of the anterior leaflet extension on the posterior leaflet gives the horizontal length r_4 and perpendicular distance h_4 of the posterior leaflet involved in mitral orifice occlusion. α_{AL} and α_{PL} = systolic leaflet coaptation angle of the anterior and posterior leaflet; D_{AL}, D_{PL} = perpendicular distance from anterior and posterior leaflet tip to the annular plane; L_{AL}, L_{PL} = horizontally projected lengths of the anterior and posterior leaflet.

tion and was used as an integrated measure for mitral leaflet tenting. The relative increase of OLA for a certain papillary muscle position in comparison with the normal condition thus reflected the severity of incomplete mitral leaflet coaptation, and may also be a reliable measure to reflect the presence of a regurgitant orifice area (see below). Occlusional leaflet area was calculated as follows. The leaflet contour of the tented leaflet configuration in a given apical scanning plane may be approximately described by four heights (h_1..h_4) and four radii (r_1..r_4) (Fig. 4). Assuming that this leaflet contour is swept through 45° of rotation about the center point of the annulus, OLA can be calculated as the sum of fractions of a cone produced from the four scanning planes, according to (modified from Boltwood et al. [9]):

$$\mathrm{OLA} = \left[\sum_{1}^{4} \frac{\pi}{8} \begin{array}{l} [(r_1 + r_2)(h_1^2 + (r_1 - r_2)^2)^{1/2} + r_2\,(r_2^2 + h_2^2)^{1/2} \\ \quad + r_3(r_3^2 + h_3^2)^{1/2} + (r_1 + (r_1 - r_4)(h_4^2 + r_4^2)^{1/2}) \\ \quad + ((r_1 - r_4) + r_3)((h_4 - (h_1 + h_2 + h_3))^2 \\ \quad + (r_1 - (r_3 + r_4))^2)^{1/2}] \end{array} \right] \quad [1]$$

in which r_4 and h_4 can be solved trigonometrically. The measure of OLA does not account for leaflet infolding or compression of leaflet tissue at the line of coaptation. Based on the equation for OLA, the occlusional leaflet area of the anterolateral and posteromedial commissural half portion of the mitral orifice (OLA_{ACOM} and OLA_{PCOM}) could easily be calculated. Line 3–4 in the equation refers to the leaflet edge separation, which by summation gives the effective regurgitant orifice area, and was canceled out in complete leaflet coaptation. However, the regurgitant orifice area itself may be difficult to assess precisely by 2D echo due to limitations of the spatial resolution.

CHORDAE AND PAPILLARY MUSCLE SPATIAL ORIENTATION. Assuming that the chordae tendineae with origin at the papillary muscle tip were inserting at the midpoint of the corresponding half mitral systolic coaptation line in early systole, the spatial orientation of the chordae connecting these coordinates could be calculated. The x,y,z coordinates of the papillary muscle tips were directly read in the spatial coordinate system of the left ventricular model. The mitral leaflet geometry assessed by 2D echo could be superimposed on this spatial coordinate system, having a well defined annular hinge and scanning planes.

From the parasternal short-axis view, the x,y coordinates of the medial and lateral midpoint of the half mitral systolic coaptation line could be identified (asterisks in Fig. 5). The transducer was then moved along the x axis to center the medial and lateral midpoint of the half mitral systolic coaptation line in the scanning planes. In these positions the transducer was rotated 90° into parasternal long-axis view, in which the z component of the midpoint of the half mitral systolic coaptation line could be measured as the distance from the leaflet tips to the annular plane.

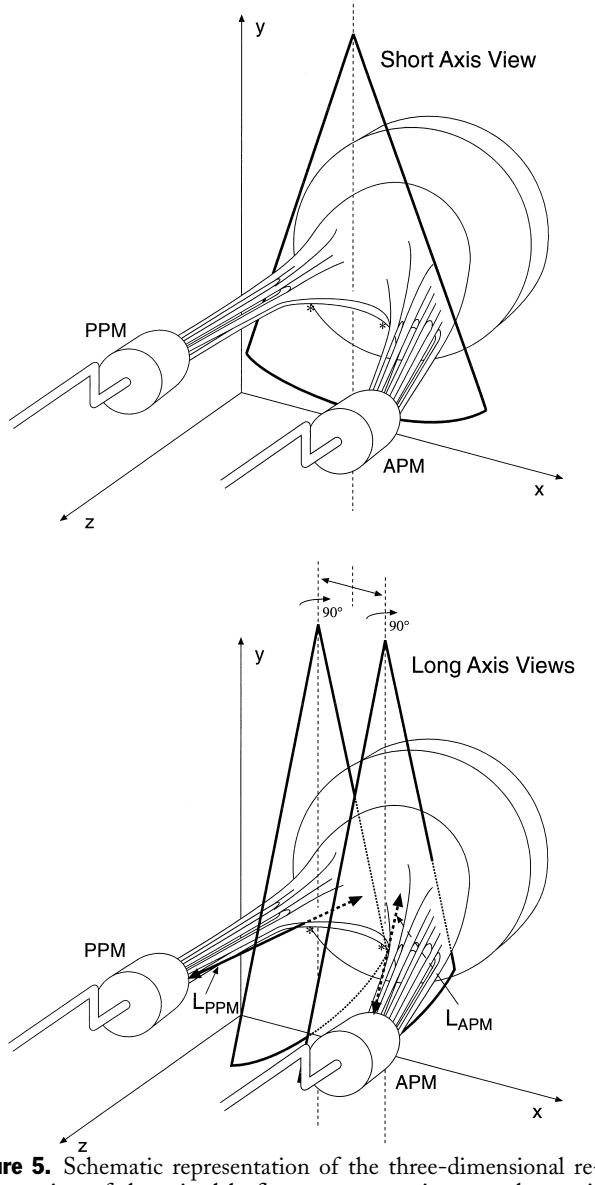

Figure 5. Schematic representation of the three-dimensional reconstruction of the mitral leaflet geometry, using one short-axis view of the annulus plane **(top)** and two parasternal long-axis views at the midpoint of the half mitral coaptation line **(bottom)**. The primary chordae connected the tip of the papillary muscles and the corresponding midpoint of the half mitral coaptation line **(asterisks)**. The central papillary muscle lines (L_{APM} and L_{PPM}) are illustrated as **double arrows** from the papillary muscle tips through the chordae attachment **(asterisks)** to the annular plane. APM = anterolateral papillary muscle; PPM = posteromedial papillary muscle.

The central papillary muscle lines (double arrows in Fig. 5) were defined between the papillary muscle tips through the corresponding midpoints of the half mitral systolic coaptation line to the annular plane. The length of the papillary muscle lines (L_{APM} and L_{PPM}) and the mean of L_{APM} and L_{PPM} (L_{PM}) designated the papillary muscle malalignment with respect to the mitral annulus.

Study Conditions

Five valves were included in the study. Alterations of the chordal force distribution were accomplished by combinations of 1) eight different papillary muscle settings (Fig. 2), 2) two peak LVP − LAP settings (90 and 150 mm Hg) and 3) two heart rate settings (70 and 120 min^{-1}). Cardiac output was kept constant at 5 liters/min or at maximum obtainable flow rate during moderate to severe MR. Two different levels of peak + (LV − LA) dP/dt were accomplished by the two heart rate settings.

Statistics

The data were analyzed using mixed models (17), which are unbalanced analysis of variance models, allowing more than one source of variation (random effects) and both nominal (valve, papillary muscle settings, high/low LVP − LAP and high/low heart rate) and continuous (e.g., L_{PM} and $\Sigma[F_C - F_T]_S$) independent variables (fixed effects). The Proc Mixed procedure in SAS was used for the analysis. Tests to determine whether the fixed effects were statistically significant were performed for each valve and for all valves at once. Significance level was $p = 0.05$.

Three different models were applied:

Model 1^{MP}. The dependent variable Y (e.g., RF) was analyzed in relation to variation in papillary muscle settings, high/low LVP − LAP and high/low heart rate:

$$Y = \alpha_{PM} + \gamma_{LVP-LAP} I_{High\ pressure} + \gamma_{HR} I_{High\ heart\ rate} + \text{error term},$$

where α_{PM} was the level for the eight papillary muscle settings, $\gamma_{LVP-LAP}$ was the difference between high/low heart rate and I_A was the indicator function equal to 1 if A was true (high pressure/heart rate) and 0 if A was false (low pressure/heart rate).

Model 2^{MP}. The dependent variable Y (e.g., RF) was analyzed in relation to variation in a continuous variable X (e.g., $\Sigma[F_C - F_T]_S$), high/low LVP − LAP and high/low heart rate:

$$Y = \alpha + \beta \cdot X + \gamma_{LVP-LAP} I_{High\ pressure} + \gamma_{HR} I_{High\ heart\ rate} + \text{error term},$$

where β was the regression coefficient of X, α the intercept and γ and I as stated above.

The range of the continuous variable X (R_X) was defined as the difference between the maximum and minimum value of X in all experiments in the same valve. Hence, the magnitude of $\beta \cdot R_X$, $\gamma_{LVP-LAP}$ and γ_{HR} indicated the contribution of X, LVP − LAP and heart rate settings to the dependent variable, Y. Due to the variation between valves, the magnitudes of β and $\beta \cdot R_X$ are stated for each valve in tables or as minimum to maximum value of five valves in the text.

Model 3^{MP}. The dependent variable Y (e.g., RF) was analyzed in relation to variation in two continuous variables X_1 and X_2 (e.g., L_{PM} and $\Sigma[F_C - F_T]_S$), high/low LVP −

Table 1. Selected Mitral Leaflet Variables in Relation to Papillary Muscle Settings

APM:PPM Settings	Mitral Leaflet Variables							
	D_{AL} (mm)	D_{PL} (mm)	φ_{AL} (°)	φ_{PL} (°)	OLA (mm^2)	OLA_{ACOM} (mm^2)	OLA_{PCOM} (mm^2)	RF
N:N	7.2 ± 0.5	10.0 ± 0.5	70 ± 1.2	39 ± 1.8	600 ± 28	304 ± 16	296 ± 13	—
A:A	9.4 ± 0.7	11.8 ± 0.5	67 ± 1.3	31 ± 1.6	685 ± 26	345 ± 15	340 ± 11	0.08 ± 0.01
N:PL	8.0 ± 0.5	12.0 ± 0.5	69 ± 1.4	26 ± 2.1	706 ± 27	354 ± 16	351 ± 13	0.11 ± 0.01
N:APL	8.4 ± 0.5	13.9 ± 0.5	67 ± 1.7	19 ± 2.1	784 ± 30	387 ± 13	397 ± 17	0.13 ± 0.02
PL:PL	7.2 ± 0.4	14.7 ± 0.5	69 ± 1.3	13 ± 1.6	843 ± 31	427 ± 17	416 ± 15	0.15 ± 0.02
PL:APL	8.4 ± 0.5	15.5 ± 0.5	67 ± 1.3	12 ± 1.9	886 ± 33	451 ± 18	436 ± 16	0.16 ± 0.02
APL:PL	7.8 ± 0.5	15.7 ± 0.6	68 ± 1.2	7 ± 1.0	939 ± 37	489 ± 21	450 ± 19	0.17 ± 0.02
APL:APL	9.7 ± 0.6	15.9 ± 0.5	64 ± 1.5	10 ± 2.1	948 ± 35	489 ± 21	459 ± 15	0.26 ± 0.04

Data are expressed as means ± SEM of four physiologic conditions for each papillary muscle setting in all valves.
A = apical; APL = apical posterolateral; APM = anterolateral papillary muscle; D_{AL}, D_{PL} = perpendicular distance from anterior and posterior leaflet tip to annular plane (apical long-axis view); N = normal; OLA, OLA_{ACOM}, OLA_{PCOM} = the total occlusional leaflet area and the anterior and posterior commissural half portion of OLA; PL = posterolateral; PPM = posteromedial papillary muscle; RF = regurgitant fraction; φ_{AL}, φ_{PL} = anterior and posterior leaflet excursion angle (apical long-axis view).

LAP and high/low heart rate, that is, the regression term $\beta \cdot X$ in model 2 was changed to $\beta_1 \cdot X_1 + \beta_2 \cdot X_2$.

The error terms in the models contained a component for each of the sources of variation: one common for the four measurements on the same valve and same papillary muscle setting (model 2 and 3), one common for two measurements (high/low LVP − LAP) in the same valve, same papillary muscle setting and same heart rate and finally a residual term.

RESULTS

With the papillary muscles mounted in normal position, 2D echocardiograms showed complete mitral leaflet coaptation with no detectable regurgitation in any of the valves at the four test conditions. The clinically observed tented leaflet geometry was successfully reproduced by papillary muscle displacement.

Determinants of leaflet configuration. Table 1 shows selected leaflet variables in relation to papillary muscle settings. Occlusional leaflet area was significantly related to papillary muscle settings ($p < 0.001$) and LVP − LAP ($p < 0.001$) (model 1^{MP}). A positive correlation was found between L_{PM} and OLA (OLA: beta = 22 to 35 [mm^2/mm], $\beta \cdot R_{LPM}$ = 261 to 552 mm^2; $p < 0.001$). Increasing LVP − LAP reduced OLA in all valves ($\gamma_{LVP-LAP} = -45$ to -10 [mm^2]; $p < 0.001$). Occlusional leaflet area was variably related to peak + (LV − LA) dP/dt (OLA: $\gamma_{HR} = -37$ to $+48$ [mm^2]).

Table 2 shows the chordal force distribution in relation to papillary muscle settings. $\Sigma[F_C - F_T]_S$ was a central factor governing variations of OLA (Table 3). A strong correlation was found between $\Sigma[F_C - F_T]_S$ and OLA (Fig. 6). Table 3 shows that the impact of LVP − LAP on OLA ($\gamma_{LVP-LAP} = -14$ to $+47$ [mm^2]; p = NS in four valves) was compensated by the variations of $\Sigma[F_C - F_T]_S$. Using $\Sigma[F_C - F_T]_S$ and L_{PM} in a covariate analysis for OLA, the significant impact of L_{PM} on OLA was entirely neutralized by variations of $\Sigma[F_C - F_T]_S$ (L_{PM}: $p = 0.46$ vs. $\Sigma[F_C - F_T]_S$: $p < 0.001$ [model 3^{MP}]).

Increasing chordal tethering forces by displacement of the papillary muscle restricted leaflet mobility tending to pull the corresponding leaflets apart. A positive correlation was found between $\Sigma[F_C - F_T]_{AL}$ and anterior leaflet excursion angle φ_{AL} (beta = 2.0 to 8.3 [°/N]; $p < 0.001$ [model 2^{MP}]) and between $\Sigma[F_C - F_T]_{PL}$ and posterior leaflet excursion angle φ_{PL} (beta = 4.7 to 12.0 [°/N]; $p < 0.001$ [model 2^{MP}]). Increasing the z component of the tethering forces by apical papillary muscle displacement significantly increased D_{AL} and D_{PL} (D_{AL} vs. $\Sigma[F_C - F_T]_{AL}[z]$: beta = -3.3 to -1.2 [mm/N], $p = 0.01$; D_{PL} vs. $\Sigma[F_C - F_T]_{PL}[z]$: beta = -3.3 to -1.3 [mm/N]; $p < 0.001$ [model 2^{MP}]). Similarly, increasing the y component of the tethering forces by posterolateral papillary muscle displacement significantly increased L_{AL} and decreased L_{PL} (L_{AL} vs. $\Sigma[F_C - F_T]_{AL}[y]$: $p < 0.01$; L_{PL} vs. $\Sigma[F_C - F_T]_{PL}[y]$: $p < 0.01$ [model 2^{MP}]).

Hence, apical papillary muscle displacement resulted in an apical shift of the leaflet coaptation line, whereas posterolateral displacement of the papillary muscles caused a remodeling of the mitral leaflet surface area in which the anterior leaflet covered a larger part of the mitral orifice, resulting in a posterior shift of the leaflet coaptation line (Fig. 7). Therefore, by posterolateral displacement of the papillary muscles the chordal coapting force component of the anterior leaflet increased due to a larger leaflet surface area disposed, which counterbalanced increasing tethering forces and thereby prevented excessive apical migration of the anterior leaflet. Leaflet infolding along the coaptation line reduced the effective posterior leaflet surface area disposed, thereby decreasing the chordal coapting force component of the posterior leaflet. Therefore, posterior leaflet mobility was restricted partly due to increasing chordal tethering forces partly due to decreasing chordal coapting forces of the posterior leaflet.

Separate changes of the posterior papillary muscle (nor-

JACC Vol. 33, No. 3, 1999
March 1, 1999:843–53

Table 2. Chordal Force Distribution in Relation to Papillary Muscle Settings

APM: PPM Settings	Chordal Force Distribution													
	$[F_T]_{AA}$	$[F_C]_{AA}$	$[F_C - F_T]_{AA}$	$[F_T]_{AP}$	$[F_C]_{AP}$	$[F_C - F_T]_{AP}$	$[F_T]_{PA}$	$[F_C]_{PA}$	$[F_C - F_T]_{PA}$	$[F_T]_{PP}$	$[F_C]_{PP}$	$[F_C - F_T]_{PP}$	$[F_T]_S$	$[F_C]_S$	$[F_C - F_T]_S$
N:N	0.00 ± 0.0	0.46 ± 0.08	0.46 ± 0.08	0.00 ± 0.0	0.45 ± 0.06	0.45 ± 0.06	0.00 ± 0.0	0.44 ± 0.0	0.44 ± 0.05	0.00 ± 0.0	0.50 ± 0.07	0.50 ± 0.07	0 ± 0.0	1.81 ± 0.19	1.81 ± 0.19
A:A	0.33 ± 0.01	0.58 ± 0.08	0.25 ± 0.07	0.55 ± 0.03	0.37 ± 0.05	−0.19 ± 0.04	0.36 ± 0.02	0.49 ± 0.06	0.12 ± 0.05	0.66 ± 0.04	0.50 ± 0.08	−0.16 ± 0.06	1.87 ± 0.07	1.89 ± 0.21	0.03 ± 0.16
N:PL	0.07 ± 0.01	0.61 ± 0.08	0.61 ± 0.08	0.13 ± 0.01	0.29 ± 0.04	0.29 ± 0.04	0.59 ± 0.03	0.59 ± 0.07	0.00 ± 0.05	1.08 ± 0.08	0.27 ± 0.04	−0.81 ± 0.07	1.67 ± 0.07	1.72 ± 0.17	0.25 ± 0.16
N:APL	0.12 ± 0.01	0.63 ± 0.08	0.51 ± 0.08	0.22 ± 0.06	0.28 ± 0.04	0.05 ± 0.08	0.80 ± 0.05	0.61 ± 0.06	−0.19 ± 0.07	1.46 ± 0.12	0.26 ± 0.04	−1.21 ± 0.09	2.59 ± 0.11	1.75 ± 0.14	−0.87 ± 0.14
PL:PL	0.48 ± 0.01	0.67 ± 0.08	0.19 ± 0.08	0.81 ± 0.04	0.15 ± 0.02	−0.65 ± 0.05	0.59 ± 0.03	0.65 ± 0.07	−0.06 ± 0.06	1.08 ± 0.08	0.28 ± 0.03	−0.81 ± 0.05	2.94 ± 0.08	1.74 ± 0.15	−1.22 ± 0.11
PL:APL	0.48 ± 0.01	0.64 ± 0.07	0.17 ± 0.07	0.81 ± 0.04	0.17 ± 0.02	−0.64 ± 0.04	0.85 ± 0.06	0.84 ± 0.08	−0.01 ± 0.07	1.53 ± 0.11	0.24 ± 0.02	−1.29 ± 0.09	3.62 ± 0.13	1.87 ± 0.13	−1.76 ± 0.18
APL:PL	0.72 ± 0.03	0.63 ± 0.08	−0.08 ± 0.06	1.14 ± 0.06	0.19 ± 0.02	−0.95 ± 0.07	0.57 ± 0.04	0.59 ± 0.06	0.02 ± 0.06	0.99 ± 0.08	0.11 ± 0.01	−0.88 ± 0.07	3.39 ± 0.06	1.51 ± 0.13	−1.90 ± 0.11
APL:APL	0.71 ± 0.02	0.72 ± 0.07	−0.14 ± 0.06	1.18 ± 0.05	0.15 ± 0.02	−1.04 ± 0.05	0.85 ± 0.06	0.81 ± 0.08	−0.03 ± 0.07	1.53 ± 0.11	0.21 ± 0.03	−1.32 ± 0.09	4.25 ± 0.14	1.88 ± 0.15	−2.37 ± 0.11

Chordal forces represented as means ± SEM (in Newtons) of four physiologic conditions for each papillary muscle setting in all valves. Chordal coapting (F_C) and chordal tethering (F_T) force components of the primary chordae are given. Subscripts refer to the location of the primary chordae.

AA = from the anterolateral papillary muscle (APM) to anterior leaflet; AP = from the anterolateral papillary muscle to posterior leaflet; PA = from the posteromedial papillary muscle (PPM) to anterior leaflet; PP = from the posteromedial papillary muscle to posterior leaflet. S = sum of the chordal force components. Other abbreviations as in Table 1.

Table 3. Impact of Chordal Force Distribution on Occlusional Leaflet Area and Mitral Regurgitant Fraction

	OLA: Independent Variables $\Sigma[F_C - F_T]_S$ (N)				
Valve	β (mm^2/N)	$\beta \cdot R_{\Sigma[F_C-F_T]_S}$ (mm^2)	$\gamma_{LVP-LAP}$ (mm^2)	γ_{HR} (mm^2)	SD (mm^2)
1	−115*	601	20	11	49
2	−82*	312	−1	48†	43
3	−76*	317	−14	47†	34
4	−79*	408	0	−19	35
5	−64*	445	47*	−43†	28
	RF: Independent Variables $\Sigma[F_C - F_T]_S$ (N)				
Valve	β (%/N)	$\beta \cdot R_{\Sigma[F_C-F_T]_S}$ (%)	$\gamma_{LVP-LAP}$ (%)	γ_{HR} (%)	SD (%)
1	−4.1*	21.6	3.2*	4.4†	2.9
2	−6.7*	25.4	3.6*	0.4	3.5
3	−1.1*	4.6	0.9†	2.1†	1.1
4	−2.5*	12.8	1.4†	1.4†	1.7
5	−6.4*	44.3	9.6*	1.7†	1.8

*$p < 0.001$. †$p < 0.05$. Occlusional leaflet area (OLA) and regurgitant fraction (RF) (dependent variables) versus total chordal net forces of the primary chordae ($\Sigma[F_C - F_T]_S$) (independent variable) using mixed procedure, model 2^{MP}. The magnitude of the regression terms (e.g., $\beta \cdot R_{\Sigma[F_C-F_T]_S}$) in comparison to $\gamma_{LVP\ -\ LAP}$ and γ_{HR} shows the relative contribution of each factor on the dependent variables. β = regression coefficient; $\gamma_{LVP\ -\ LAP}$ and γ_{HR} = difference of the dependent variable between transmitral pressure difference and heart rate settings; $R_{\Sigma[F_C-F_T]_S}$ = range of $\Sigma[F_C - F_T]_S$ (maximum − minimum value of all experiments in one valve); SD = standard deviation (square root of the sum of three variance components).

mal:PL, normal:APL papillary muscle settings) increased $[F_T]_{PA}$ and $[F_T]_{PP}$ and also caused a reduction of the chordal coapting forces of the posterior leaflet on both sides of the commissures ($[F_C]_{AP}$ and $[F_C]_{PP}$) (Table 2). Posteromedial papillary muscle displacement thus affected the corresponding half portion of occlusional leaflet area, OLA_{PCOM}, but tended also to increase OLA_{ACOM}, even though the anterolateral papillary muscle position was unchanged (Table 1).

Determinants of regurgitant fraction. Mitral regurgitant fraction significantly increased with papillary muscle displacement ($p < 0.001$, model 1^{MP}). Apical papillary muscle displacement was sufficient to create MR; however, posterolateral and apical posterolateral displacement was necessary to create more important and clinically significant MR (Table 1). Increasing LVP − LAP tended to increase RF ($\gamma_{LVP\ -\ LAP} = -0.03$ to $+3.9$ [%]; $p < 0.001$), even though that LVP − LAP caused a reduction of OLA. In four of five valves, RF was virtually unaffected by changes of heart rate ($\gamma_{HR} = 0.2$ to 2.4 [%], p = NS). Only in one valve was RF significantly higher at heart rate of 120 min^{-1} than of 70 min^{-1} ($\gamma_{HR} = 5.1$ [%], $p < 0.001$). However, RF may be affected by the relative systolic and diastolic duration, which was not fully comparable in the two heart rate settings. In contrast, the early systolic precoaptation regurgitant volume was actually significantly reduced with increasing heart rate ($\gamma_{HR} = -0.06$ to -0.008 [liter]; $p < 0.001$, Model 1^{MP}).

Using regression analysis (model 2^{MP}), RF was closely

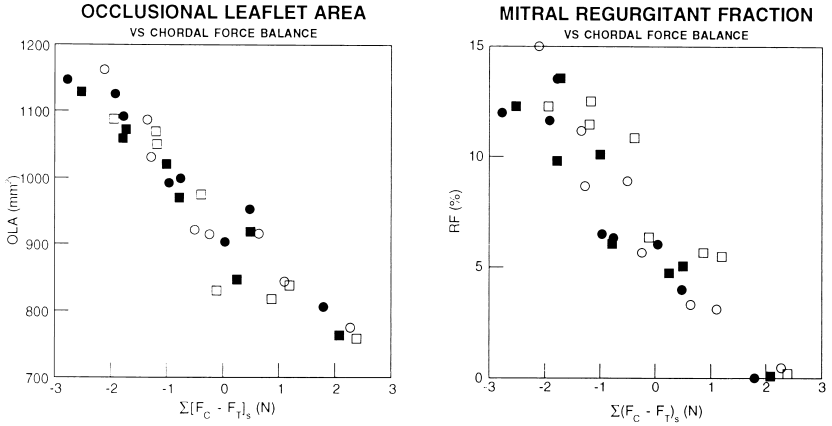

Figure 6. A linear correlation was demonstrated between the occlusional leaflet area (OLA) and regurgitant fraction (RF) (dependent variables) and the total chordal netforces, $\Sigma[F_C - F_T]_S$ (independent variable). Data represent one valve at all test conditions. Trends are representative of all valves (compare with Table 3). **Solid circles** = HR: 70; LVP − LAP: 90; **solid squares** = HR: 120; LVP − LAP: 90; **open circles**: HR: 70; LVP − LAP: 150; **open squares** = HR: 120; LVP − LAP: 150. HR = heart rate; LVP − LAP = transmitral pressure difference.

related to variations of $\Sigma[F_C - F_T]_S$ (Table 3 and Fig. 6) as well as OLA (beta = 0.014 to 0.091 [%/mm^2]; $p < 0.001$).

DISCUSSION

By application of the premise of the chordal force balance, incomplete mitral leaflet coaptation can be a result of: 1) abnormally increased tension caused by displacement of the annular (9) and papillary muscle attachment (3–8) and 2) decreased global left ventricular systolic function, decreasing the coapting forces to close the mitral leaflets (5,7,18).

Our study emphasizes that redistribution of the chordal force balance leads to incomplete mitral leaflet coaptation.

Papillary muscle malalignment increased the chordal tethering forces and induced functional MR based on the tented leaflet configuration as observed clinically (3).

Increasing chordal tethering forces restricted leaflet mobility, impeded mitral valve coaptation and increased regurgitation. In addition, redirection of the chordal force components by a posterolateral shift of the papillary muscles caused a remodeling of the mitral leaflet surface area. This process can be interpreted as follows. Increased tethering forces in posterior direction restricted posterior leaflet excursion angle. Leaflet separation was partly compensated by the anterior leaflet covering a larger part of the mitral valve orifice. Therefore, the mitral leaflet coaptation line moved in an apical and posterior direction in an asymmetrical coaptation pattern, which has also been reported clinically (10). As a consequence, the coapting forces of the anterior leaflet increased due to exposure of a larger leaflet surface area. Thereby, excessive apical migration of the anterior leaflet was prevented. Conversely, a reduction of the posterior leaflet surface area due to leaflet infolding caused less coapting force to counterbalance increasing tethering forces, resulting in further leaflet malalignment (compare Fig. 7). The anatomical substrate for anterior leaflet expansion may be unfolding of the leaflet tissue at the coaptation zone (rough zone) and stretching due to horizontal stress.

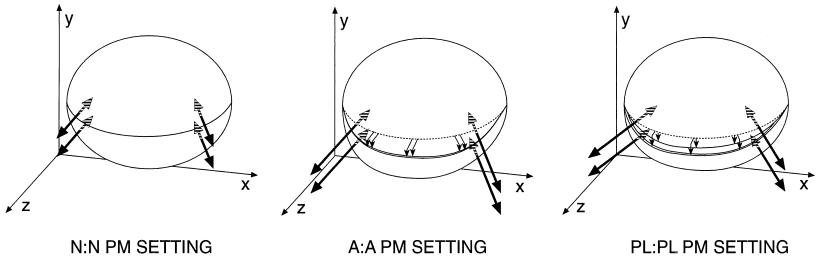

Figure 7. Diagram showing mitral leaflet remodeling **(thin arrows)** caused by redistribution of the chordal tethering **(thick black arrows)** and coapting forces **(dotted arrows)** during apical (A) and posterolateral (PL) papillary muscle (PM) displacement. Apical displacement of the papillary muscles resulted in an apical shift of the leaflet coaptation line. Posterolateral displacement of the papillary muscles caused a posterior shift of the leaflet coaptation line. Therefore, the chordal coapting force component of the anterior leaflet increased, generating a nonuniform regurgitant orifice area. N = normal.

Lateralization of the chordal tethering forces might have exacerbated the degree of incomplete mitral leaflet coaptation by diverting the central parts of the leaflets away from closure (8).

Recent clinical studies of functional MR have shown early and late systolic peaks in mitral regurgitant flow and regurgitant orifice area, which decreases in midsystole coinciding with maximum transmitral pressure difference (19). A possible explanation for this phenomenon includes increased left ventricular pressure, which closes the leaflets more effectively. This mechanism was partly supported by our data, which demonstrated that increasing chordal coapting forces by changing the left ventricular pressure reduced OLA. However, any favorable reduction of the regurgitant orifice area for a given subvalvular geometry was counteracted by increasing regurgitant flow velocities causing the observed increase of regurgitant volume to driving pressure.

Increasing peak + (LV − LA) dP/dt in early systole was associated with a reduction of the precoaptation regurgitant volume, indicating accelerated mitral leaflet coaptation and a relative delay of fluid momentum. However, increasing peak + (LV − LA) dP/dt did not cause more effective closure of the mitral leaflets (OLA insensitive to peak + [LV − LA] dP/dt). Therefore, we do not consider a slow rate of rise of pressure, as speculated by Kaul et al. (5), to be a primary determinant of incomplete mitral leaflet coaptation and functional MR.

Using three-dimensional echocardiography to explore geometric determinants of functional MR in a canine model of global left ventricular dysfunction, Otsuji et al. (8) showed that MR occurred in relation to increased papillary muscle-to-annulus tethering length after papillary muscle displacement in lateral and posterior direction rather than in apical direction along the left ventricular long axis. In agreement with our findings, it was suggested that a lateral and posterior shift of the papillary muscles redirects papillary muscle tension away from the axial direction, diverting the leaflets away from closure. Our in vitro study elucidated this issue further by demonstrating decreased coapting forces of the posterior leaflet due to leaflet remodeling that enhanced leaflet malalignment.

Recent studies in our own laboratory have shown that annular dilation was a necessary condition to generate more significant levels of MR (13). However, annular dilation was not sufficient to develop the tented leaflet geometry without papillary muscle displacement. Therefore, in the present study we kept mitral annular dimension constant to demonstrate that altered chordal force distribution accomplished by papillary muscle displacement reproduces tented mitral leaflet configuration and functional MR as observed clinically.

Functional MR appears in an orchestra of geometric and hemodynamic variables that accompany acute and chronic left ventricular dysfunction. The chordal force distribution is the key factor, which mediates the relative contribution and interaction of these variables, and thereby determines systolic mitral leaflet configuration.

Model considerations. Previous in vivo studies of these mechanistic factors of functional MR have provided data of limited value for two reasons. First, proposed causes of MR could not be deliberately varied to show that they induced regurgitation in an initially competent valve (11). Second, competing hemodynamic and geometric factors could not be readily separated in vivo (5). Our in vitro model allowed us to test these interactions; to show that postulated changes, in fact, can induce regurgitation in this model, and to demonstrate their overall similarity to clinical observations.

Normally, the mitral valve acts as an integrated system, with dynamic changes in the relation between the annulus and papillary muscle–chordae tendinae complex that permit efficient closure throughout the systole (20). The model reproduced at different time steps of the cardiac cycle the instantaneous papillary muscle and annular relationships that occur with akinetic or dyskinetic function of the left ventricular posterior wall (13). Although the dynamic changes of the left ventricle as a whole were not simulated, the pressure and flow changes were. The fixation of the papillary muscles to mounting rods even allowed us to separate the chordal coapting forces and the tethering forces in the chordal force measurements, which would be impossible to accomplish in vivo.

Clinical implications. Even though any clinical implications of this model must be stated circumspectly, this in vitro study can potentially help us to gain insight into therapeutic interventions that modify mechanistic factors, for example, the role of new surgical approaches that can modify the geometric relationships, such as chordal reconstruction (21), papillary muscle repositioning (20,22) and resection of posterior wall myocardium between the papillary muscles to move them closer together (23). Our study indicates that remodeling of the mitral valve substructures (e.g., chordal lengthening) may be a relevant surgical approach to "normalize" the chordal force distribution in functional MR. However, one may be aware that chordal lengthening itself, instead of "slackening the reins" of the mitral leaflets, may adversely deteriorate left ventricular function due to loss of support of the left ventricular wall (valvular–ventricular interaction). Therefore, surgical correction could involve lengthening of the primary chordae, possibly in combination with transposition or shortening of the secondary (strut) chordae with the aim of improving mitral valve function and interaction with the left ventricle. Further studies on this issue are in progress.

Acknowledgment

We thank the AV Department, Aarhus University Hospital for artistic illustrations.

Reprint requests and correspondence: Sten Lyager Nielsen, MD, Department of Cardiothoracic and Vascular Surgery, Skejby Sygehus, Aarhus University Hospital, 8200 Aarhus N, Denmark.

REFERENCES

1. Frantz E, Weininger F, Oswald H, Fleck E. Predictors for mitral regurgitation in coronary artery disease. In: Vetter HO, Hetzer R, Schmutzler H, editors. Ischemic Mitral Incompetence. New York: Springer-Verlag, 1991:57–73.
2. Lehmann KG, Francis CK, Dodge HT. Mitral regurgitation in early myocardial infarction. Incidence, clinical detection, and prognostic implications. TIMI Study Group. Ann Intern Med 1992;117:10–7.
3. Godley RW, Wann LS, Rogers EW, Feigenbaum H, Weyman AE. Incomplete mitral leaflet closure in patients with papillary muscle dysfunction. Circulation 1981;63:565–71.
4. Burch GE, DePasquale NP, Phillips JH. The syndrome of papillary muscle dysfunction. Am Heart J 1968;75:399–415.
5. Kaul S, Spotnitz WD, Glasheen WP, Touchstone DA. Mechanism of ischemic mitral regurgitation. An experimental evaluation. Circulation 1991;84:2167–80.
6. Kono T, Sabbah HN, Rosman H, Alam M, Jafri S, Goldstein S. Left ventricular shape is the primary determinant of functional mitral regurgitation in heart failure. J Am Coll Cardiol 1992;20:1594–8.
7. Kono T, Sabbah HN, Rosman H, et al. Mechanism of functional mitral regurgitation during acute myocardial ischemia. J Am Coll Cardiol 1992;19:1101–5.
8. Otsuji Y, Handschumacher MD, Schwammenthal E, et al. Insights from three-dimensional echocardiography into the mechanism of functional mitral regurgitation: direct in vivo demonstration of altered leaflet tethering geometry. Circulation 1997;96:1999–2008.
9. Boltwood CM, Tei C, Wong M, Shah PM. Quantitative echocardiography of the mitral complex in dilated cardiomyopathy: the mechanism of functional mitral regurgitation. Circulation 1983;68:498–508.
10. Izumi S, Miyatake K, Beppu S, et al. Mechanism of mitral regurgitation in patients with myocardial infarction: a study using real-time two-dimensional Doppler flow imaging and echocardiography. Circulation 1987;76:777–85.
11. Gorman RC, McCaughan JS, Ratcliffe MB, et al. Pathogenesis of acute ischemic mitral regurgitation in three dimensions. J Thorac Cardiovasc Surg 1995;109:684–93.
12. Salisbury PF, Cross CE, Rieben PA. Chorda tendinea tension. Am J Physiol 1963;205:385–92.
13. He S, Fontaine AA, Schwammenthal E, Yoganathan AP, Levine RA. Integrated mechanism for functional mitral regurgitation. Leaflet restriction vs coapting force: in vitro studies. Circulation 1997;96:1826–34.
14. Brock RC. The surgical and pathological anatomy of the mitral valve. Br Heart J 1952;14:489–513.
15. Kunzelman KS, Cochran RP. Mechanical properties of basal and marginal mitral valve chordae tendineae. ASAIO Trans 1990;36:M405–8.
16. Yacoub M. Anatomy of the mitral valve chordae and cusps. In: Kalmonson D, editor. The Mitral Valve. A Pluridisciplinary Approach. London: Edward Arnold, 1976:15–20.
17. Littell RC, Milliken GA, Stroup WW, Wolfinger RD. SAS© System for Mixed Models. Cary, NC: SAS Institute Inc., 1996:491–504.
18. Tsakiris AG, Gordon DA, Padiyar R, Frechette D. Relation of mitral valve opening and closure to left atrial and ventricular pressures in the intact dog. Am J Physiol 1978;234:H146–51.
19. Schwammenthal E, Chen C, Benning F, Block M, Breithardt G, Levine RA. Dynamics of mitral regurgitant flow and orifice area. Physiologic application of the proximal flow convergence method: clinical data and experimental testing. Circulation 1994;90:307–22.
20. Frater RWM, Cornelissen P, Sisto D. Mechanisms of ischemic mitral insufficiency and their surgical corrections. In: Vetter HO, Schmultzer H, editors. Ischemic Mitral Incompetence. New York: Springer Verlag, 1991:117–30.
21. Komeda M, Glasson JR, Bolger AF, et al. Geometric determinants of ischemic mitral regurgitation. Circulation 1997;96 Suppl II:II-128–33.
22. Liel-Cohen N, Guerrero JL, Otsuji Y, et al. Insights from three-dimensional echocardiography: design of a new surgical approach for ventricular remodeling to relieve ischemic mitral regurgitation (abstr). J Am Coll Cardiol 1998;31 Suppl: 410–5.
23. McCarthy PM, Starling RC, Wong J, et al. Early results with partial left ventriculectomy. J Thorac Cardiovasc Surg 1997; 114:755–63.